JOURNAL OF CATALYSIS **171,** 160–168 (1997)
ARTICLE NO. CA971784

Effects of Trivalent Dopants on the Redox Properties of $Ce_{0.6}Zr_{0.4}O_2$ Mixed Oxide

Polona Vidmar,[1] Paolo Fornasiero, Jan Kašpar,[2] Giuseppe Gubitosa,* and Mauro Graziani

*Dipartimento di Scienze Chimiche, Università di Trieste, Via Giorgieri 1, 34127 Trieste, Italy; and *Magneti Marelli D.S.S., V.le Carlo Emanuele II, 150, 10078 Venaria Reale, Turin, Italy*

Received February 3, 1997; revised May 13, 1997; accepted May 31, 1997

We have observed that the insertion of trivalent cations into the lattice of $Ce_{0.6}Zr_{0.4}O_2$ solid solution improves the oxygen storage capacity at low temperatures by decreasing the temperature of the reduction in the bulk of the solid solution compared to the undoped sample. The effect depends on the type of dopant and its concentration. Reduction of the solid solution at moderate temperatures is strongly improved upon aging in H_2/Ar independently of the extensive sintering of the sample.

INTRODUCTION

CeO_2 is present in the majority of the formulations of the three-way catalysts (TWC) due to its well-known multiple effects on the catalyst state and performance: (i) oxygen storage and release capacity (OSC); (ii) stabilization of metal dispersion; (iii) promotion of the water gas shift reaction. The role of CeO_2 as an efficient "oxygen buffer" is directly related to its capability to undergo effective reduction and reoxidation under rich and lean conditions, respectively. By storing and releasing oxygen, CeO_2 keeps the reductant/oxidant ratio in the exhaust close to the stoichiometric value where the highest conversions of all the pollutants are attained (1, 2). Moreover, transient but highly productive exhaust conversion was observed for reduced CeO_2 containing TWCs (3). All these factors point to the importance of the Ce^{4+}/Ce^{3+} redox couple in improving the TWCs performances. A major drawback of CeO_2 is that significant deactivation of the redox couple occurs due to sintering of the CeO_2 particles when it is used at high temperature in the driving conditions (4). A great number of CeO_2-based systems (e.g., CeO_2–Al_2O_3 (5), CeO_2–SiO_2 (6), CeO_2–La_2O_3 (5), CeO_2–HfO_2 (7)) have been examined with the aim of increasing the thermal stability of CeO_2 and preventing the decline of OSC. We investigated the CeO_2–ZrO_2 solid solutions extensively and have shown that by structural doping of CeO_2 with ZrO_2, it is possible to obtain systems of very high OSC due to the occurrence of reduction in the bulk of the solid solution at moderate temperatures (8). Remarkably, this property allows us to maintain the high OSC in these systems even after drastic sintering (9). We have also tested the catalytic efficiency of these systems as model TWCs. The metal-loaded CeO_2–ZrO_2 solid solutions have shown a high catalytic activity for the NO + CO reaction (10). We also observed that a gradient of oxygen vacancies generated in the bulk of the solid solution by a reduction, induces a NO reduction at expense of the Ce^{4+}/Ce^{3+} redox couple (11). This points out the importance of improving the reducibility of the mixed oxide in the bulk.

The aim of the present work is to investigate the influence of trivalent dopants on the redox properties of the CeO_2–ZrO_2 system. It is well known that fluorite type oxides of IV group elements containing low-valent cations are good ionic conductors, frequently used as electrochemical oxygen pumps.

The stability of the redox properties against thermal treatments was also investigated since a close coupled location of the converter is nowadays employed in the automotive applications where the TWCs reach temperatures up to 1200 K.

Our previous study showed that among the $Ce_mZr_{1-m}O_2$ ($m = 0.1$–0.9) solid solutions investigated, those with the highest ZrO_2 content compatible with a cubic symmetry showed the best redox properties and the highest OSC (8). The phase transition from the tetragonal $Ce_mZr_{1-m}O_2$ to the cubic phase is located close to $m = 0.6$ even if, due to its metastable nature (9, 12, 13), an exact location of this boundary is still a matter of debate. Here we have synthesized high surface area $Ce_{0.6}Zr_{0.4-x}M_xO_{2-x/2}$ ($M = Y^{3+}$, La^{3+}, Ga^{3+}, $x = 0.01$–0.10) and investigated their redox properties.

EXPERIMENTAL

The $Ce_{0.6}Zr_{0.4-x}M_xO_{2-x/2}$ mixed oxides ($M = Y^{3+}$, La^{3+}, Ga^{3+}) were synthesized from nitrate precursors by

[1] On leave from J. Stefan Institute, P.O.B. 100, 1001 Ljubljana, Slovenia.
[2] Corresponding author. Fax: +39-40-6763960. E-mail: kaspar@univ.trieste.it.

0021-9517/97 $25.00

TABLE 1

Textural Properties and Particle Size of $Ce_{0.6}Zr_{0.4-x}M_xO_{2-x/2}$

Sample	Chemical composition	S_t surface area[a] ($m^2\ g^{-1}$)	Micropore volume ($cc\ g^{-1}$)	Average particle size (nm)[b] 773 K[c]	1273 K[d]	1273 K[e]
	$Ce_{0.6}Zr_{0.4}O_2$	89	0.031	5.1	13.9	14.8
Y(1)	$Ce_{0.6}Zr_{0.39}Y_{0.01}O_{1.995}$	79	0.027	5.0	14.7	15.5
Y(2.5)	$Ce_{0.6}Zr_{0.375}Y_{0.025}O_{1.9875}$	98	0.035	4.8	17.9	15.6
Y(5)	$Ce_{0.6}Zr_{0.35}Y_{0.05}O_{1.975}$	103	0.036	5.2	19.9	16.4
Y(10)	$Ce_{0.6}Zr_{0.30}Y_{0.10}O_{1.95}$	111	0.039	4.8	19.1	17.8
La(2.5)	$Ce_{0.6}Zr_{0.375}La_{0.025}O_{1.9875}$	111	0.040	4.6	16.2	17.2
Ga(2.5)	$Ce_{0.6}Zr_{0.375}Ga_{0.025}O_{1.9875}$	91	0.032	4.7	22.4	17.4

[a] S_t calculated from the *t*-plot.
[b] Estimated by the line broadening method.
[c] Fresh samples.
[d] Samples, calcined at 1273 K for 5 h.
[e] Aged samples.

complexing the cations with the citrate (14). In the following text, the doped samples will be denoted by the symbol of the dopant and its concentration in the brackets (compare Table 1). In short the preparation is carried out as follows. After dissolving $Ce(NO_3)_3 \cdot 6H_2O$ (41.15% CeO_2, Aldrich) and $ZrO(NO_3)_2 \cdot xH_2O$ (35.58% ZrO_2, Aldrich) in methanol (99.8%, AnalaR), the solutions of the dopant's salt ($Y(NO_3)_3 \cdot 5H_2O$; 99.9%, Aldrich; $La(NO_3)_3 \cdot 6H_2O$; 99.99%, Merck–Schuchardt; $Ga(NO_3)_3 \cdot 8H_2O$; 99.99%, Fluka) and of citric acid (99.7%, Prolabo) in methanol were added. The resulting solution was stirred at room temperature for at least 12 h. The solvent was then eliminated using a rotary evaporator. First, a transparent gel occurred and after the evolution of nitrogen oxides, a solid was obtained. This was flash decomposed at 773 K and then calcined at this temperature for 5 h to obtain a yellow powder. Hereafter these samples are indicated as fresh ones.

Powder X-ray diffraction patterns were collected on a Siemens Kristalloflex Mod.F Instrument (Ni-filtered Cu$K\alpha$). Cell parameters were determined by using the TREOR90 program which employs the Visser algorithm. The peak deconvolution was carried out after the subtraction of contribution of the $K\alpha_2$ line to the spectrum. Pearson VII functions were employed for the peak deconvolution. Rietwield analysis was carried out by using the RIETAN-94 program. FT-Raman spectra were performed on a Perkin Elmer 2000 FT-Raman instrument with diode pumped YAG laser and a room temperature super InGaAs detector. The laser power was 500–600 mW. N_2 adsorption isotherms at 77 K were obtained on a Micromeritics ASAP 2000 analyzer.

Temperature programmed reduction (TPR) was carried out as previously described (9). In order to minimize the contribution of adsorbed species, prior to TPR analysis, the sample (0.05 g) was heated in a flow of Ar up to 900 K, for 5 h. A typical reduction was carried out in a mixture Ar + 5% H_2 up to a temperature of 1273 K which was maintained for 15 min. The heating rate was 10 K min^{-1}. H_2 consumption in the TPR experiment was estimated from the integrated peak areas by comparison with those obtained by using CuO as a standard. After the TPR, the sample was outgassed under an Ar flow at 1273 K for 30 min and cooled in approximately 15 min down to 700 K, where the O_2 uptake was measured by a pulse technique. Pulses of O_2 (0.092 ml) were injected into the flow of Ar passing over the sample until the breakthrough point was attained. In order to investigate the effects of aging on the redox properties of the samples, the above described TPR/oxidation cycle was typically repeated four times. Afterwards, the samples were subjected to a new TPR up to a selected temperature (650, 750, and 850 K) and reduced for 2 h at this temperature. Hereafter this treatment will be referred to as "isothermal reduction," since the major contribution to the reduction is due to prolonged exposition in the H_2 mixture at constant temperature. The samples were then cooled (or heated) to 700 K in Ar flow, H_2 desorbed for 1 h and the O_2 uptake measured. Samples obtained from these treatments, hereafter are indicated as "aged" ones. A final TPR up to 1273 K was recorded on the aged samples.

RESULTS

Characterization of the Fresh Samples

The chemical composition and the textural properties of the undoped and doped CeO_2–ZrO_2 solid solutions investigated in this work are summarized in Table 1. The influence of the amount of inserted trivalent dopant was investigated for Y^{3+} while the dependence on the nature of the dopant was studied at a dopant loading of 2.5 mol%. All the samples show relatively high surface area. Except for the Ga(2.5) sample, a dopant content equal to or higher than 2.5 mol% favors an increase of surface area compared to both the undoped and 1 mol% Y^{3+} doped sample. For all the samples N_2 isotherms of type IV with a hysteresis of type H_2 were obtained. The presence of microporosity was detected. The surface areas were therefore calculated by the *t*-method (Table 1). The micropore volumes slightly increase from 0.027 to 0.040 ml g^{-1} as the surface area increases from 79 to 111 $m^2\ g^{-1}$, respectively (Table 1), as calculated from the desorption isotherms by the Dubinin–Radushkevich method. Accordingly, the total pore volume increases from 0.067 to 0.084 cc g^{-1} as evaluated from Gurtvich rule. The similarity of the texture of all the samples clearly points out that the textural properties are related to the synthesis conditions rather than to a particular composition.

The powder X-ray pattern of the fresh $Ce_{0.6}Zr_{0.4}O_2$ is shown in Fig. 1, trace 1. It features broad symmetric peaks attributed to the presence of small crystallites which are

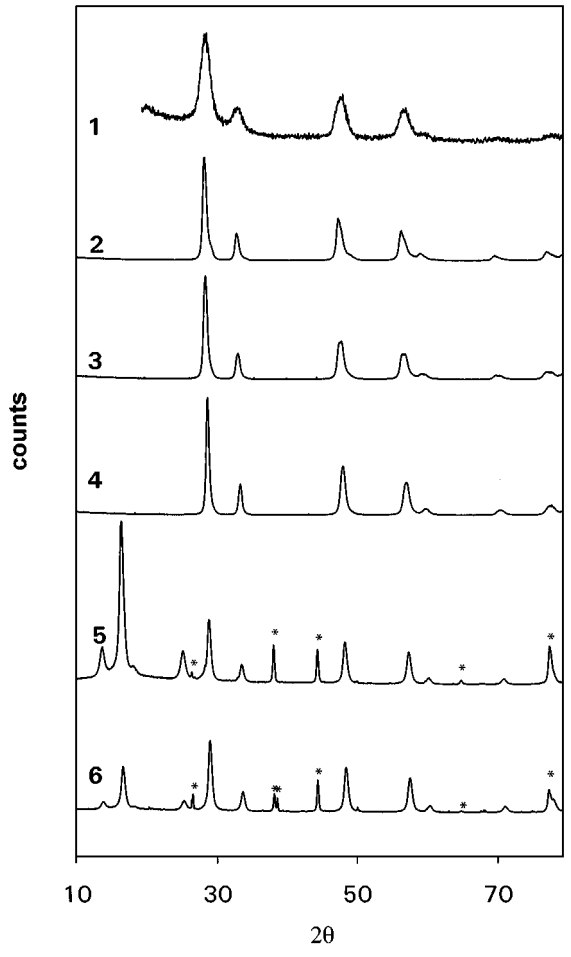

FIG. 1. Powder XRD patterns of: (1) fresh $Ce_{0.6}Zr_{0.4}O_2$; (2) $Ce_{0.6}Zr_{0.4}O_2$ calcined at 1273 K; (3) $Ce_{0.6}Zr_{0.39}Y_{0.01}O_{1.995}$ calcined at 1273 K; (4) $Ce_{0.6}Zr_{0.375}Y_{0.025}O_{1.9875}$ calcined at 1273 K; (5) aged $Ce_{0.6}Zr_{0.375}Y_{0.025}O_{1.9875}$; (6) aged $Ce_{0.6}Zr_{0.4}O_2$. The peaks marked with * are due to quartz or Al holder.

formed after the calcination at 773 K. Similar profiles were also obtained for the other samples. An estimate of the average particle sizes obtained by the line broadening method is given in Table 1. The relatively constant value around 5 nm observed for the fresh samples is in agreement with the observation that the initial texture and also particle size are strictly related to the method of synthesis. The width of the XRD peaks does not allow unequivocal assignment of the reported pattern to a *cubic* phase since the presence of the tetragonal (t') phase is usually detected by broadening and splitting of the peaks observed in CeO_2 at about 47° and 59° (2θ) which are indexed respectively as (220) and (222) planes in the Fm3m space group (12). We recall, that three different tetragonal phases (t, t', and t'') were reported for the ceria-zirconia system which can be distinguished on the basis of XRD and Raman spectra (13, 15, 16). Of these, the t-form is a stable one formed through a diffusional phase decomposition, the t'-form is obtained through a diffusionless transition and is metastable, while the t''-form is intermediate between t' and c. It shows no tetragonality and it exhibits an oxygen displacement from ideal fluorite sites (13). The t'' phase is generally referred as a *cubic* phase because its XRD pattern is indexed in the cubic Fm3m space group. This is due to the fact that the XRD pattern is generated essentially by the cation sublattice. Consistently, we refer the term *cubic* both to c and t'' phase.

All the samples were calcined at 1273 K for 5 h and the nature of the phase examined. Selected XRD patterns are reported in Fig. 1. The width of all the XRD peaks decreases upon calcination at 1273 K, which is an indication that sintering of the samples occurred (compare Fig. 1, traces 1 and 2). The average particle sizes of the calcined samples are reported in Table 1. The resulting particle size depends on the nature and the amount of the dopant. Except for the Y(10), an increase of the Y^{3+} dopant favors the sintering of the powders. Generally speaking, the presence of surface vacancies increases the rate of sintering, which might suggest that some Y^{3+} may be located also on the surface. As discussed below, for the highest (10 mol%) Y^{3+} content, Y_2O_3 separation is favored which may account for the somewhat lower particle size compared to the 5 mol% loaded sample.

Note that after calcination at 1273 K, the powder XRD pattern shows a visible tailing at the high 2θ; see, for example, the (111), (220), and (222) reflections (at about 29°, 48°, and 60°, (2θ)) in both the $Ce_{0.6}Zr_{0.4}O_2$ and Y(1). This suggests the presence of a mixture of two phases and some tetragonality of the obtained phase as suggested by the splitting of the (311) and (400) reflections at about 70° and 80° (2θ). Only, after increasing the dopant amount to and above 2.5 mol%, the symmetry of the peak profiles increases which indicates that formation of a single phase is favored (Compare Fig. 1, traces 2, 3, and 4). This phase is indexed in the Fm3m space group according to Meriani and Spinolo (12). No evidence for extra peaks due to nonincorporated Y_2O_3 was found in any XRD spectrum of both the fresh and calcined samples, suggesting that the citrate route employed in the present syntheses provides an efficient route of incorporating the dopant cations in the host lattice. Formation of a single homogeneous *cubic* phase is confirmed by the Rietwield analysis of the XRD profile of the calcined Y(2.5). The comparison of the calculated and the experimental profiles is reported in Fig. 2. The obtained cell parameter of $a = 5.3256(6)$ Å compares well with the value of 5.312 Å calculated upon application of the Vegards rule according to Ref. (17).

La^{3+} also effectively stabilises the cubic phase and a single *cubic* phase is detected in the La(2.5) after calcination at 1273 K. Similarly, about 80% of *cubic* phase is detected in the Ga(2.5), the remaining is the tetragonal t' phase.

The Raman spectra of the fresh samples appear very similar: they exhibit a strong peak at about 475 cm^{-1} and two

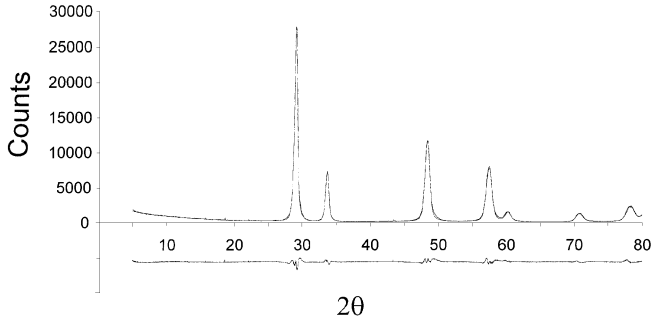

FIG. 2. Profile-fitting patterns of the $Ce_{0.6}Zr_{0.375}Y_{0.025}O_{1.9875}$ calcined at 1273 K. The profile of the sample was deconvoluted using the Fm3m symmetry (cations in the statistical occupancy). The reliability factors are: Rp = 5.6% and Rwp = 8.3%. Fitting results: $a = 5.3256(6)$ Å, density 5.35 g cm^{-3}.

weak features at 307 and 125 cm^{-1} as exemplified in Fig. 3 for $Ce_{0.6}Zr_{0.4}O_2$ and Y(2.5). The patterns suggest some distortion of the oxygen lattice which is consistent with the presence of t'' phases. After calcination at 1273 K, the width of the peak at 475 cm^{-1} decreases due to the sample sintering (18). No additional peaks are observed, suggesting that no detectable structural modification occurred and that the t'' symmetry was conserved.

Reduction Behaviour and Oxygen Uptake

The TPR profiles of the fresh samples are plotted in Fig. 4. To eliminate the contribution of the adsorbed carbonates to the TPR profile, all samples were thermally treated before the first TPR experiment following the standard procedure described in the experimental (9). Such a treatment leads to a small reduction of the sample (<3% of Ce^{4+}); however, this does not modify the TPR profiles of the fresh samples as confirmed by separate experiments in which an oxidation at 700 K and an O_2 desorption step were included in the pretreatment procedure.

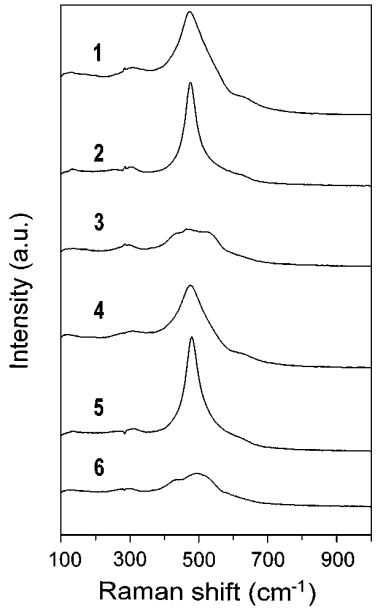

FIG. 3. Raman spectra of: (1) fresh $Ce_{0.6}Zr_{0.4}O_2$; (2) $Ce_{0.6}Zr_{0.4}O_2$ calcined at 1273 K; (3) aged $Ce_{0.6}Zr_{0.4}O_2$; (4) fresh $Ce_{0.6}Zr_{0.375}Y_{0.025}O_{1.9875}$; (5) $Ce_{0.6}Zr_{0.375}Y_{0.025}O_{1.9875}$, calcined at 1273 K; (6) aged $Ce_{0.6}Zr_{0.375}Y_{0.025}O_{1.9875}$.

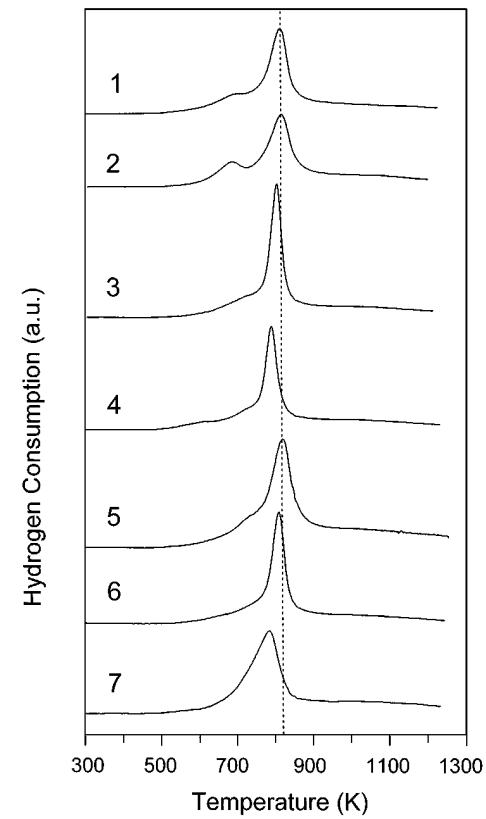

FIG. 4. Temperature programmed reduction of fresh (1) $Ce_{0.6}Zr_{0.4}O_2$; (2) $Ce_{0.6}Zr_{0.39}Y_{0.01}O_{1.995}$; (3) $Ce_{0.6}Zr_{0.375}Y_{0.025}O_{1.9875}$; (4) $Ce_{0.6}Zr_{0.35}Y_{0.05}O_{1.975}$; (5) $Ce_{0.6}Zr_{0.35}Y_{0.10}O_{1.95}$; (6) $Ce_{0.6}Zr_{0.375}La_{0.025}O_{1.9875}$; (7) $Ce_{0.6}Zr_{0.375}Ga_{0.025}O_{1.9875}$.

The fresh $Ce_{0.6}Zr_{0.4}O_2$ mixed oxide features a peak at 822 K with a shoulder at 700 K (Fig. 4, trace 1). This shape is not modified by doping the system with 1 mol% Y^{3+} (Fig. 4, trace 2). By increasing the Y^{3+} content up to 5 mol% (Fig. 4, traces 3, 4), the maximum of the peak shifts down to 796 K while the contribution of the shoulder at about 700 K becomes smaller, compared to the undoped and 1 mol% doped sample. At a constant dopant concentration (2.5 mol%) (Fig. 4, traces 4, 6, 7), the reduction profiles are very similar. The reduction temperature increases to 813 K in the case of the La(2.5), while the broad feature observed for the Ga^{3+} containing sample is shifted down to 785 K (Fig. 4, trace 7).

The redox properties of both CeO_2 and $Ce_{0.5}Zr_{0.5}O_2$ are strongly related to texture, which is modified by thermal

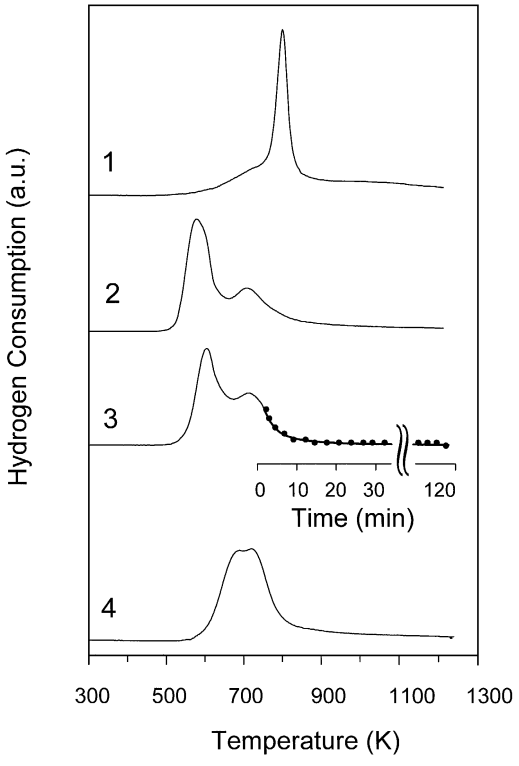

FIG. 5. Temperature programmed reduction of $Ce_{0.6}Zr_{0.375}Y_{0.025}O_{1.9875}$: (1) fresh sample; (2) sample recycled from three consecutive TPRs up to 1273 K and subsequent oxidations at 700 K; (3) TPR up to 750 K followed by isothermal reduction for 2 h of sample recycled from (2); (4) TPR of sample recycled from (3).

treatments (9). We have therefore investigated the influence of subsequent TPR/oxidation experiments on the reduction behaviour (see experimental section). A typical sequence of the TPR profiles obtained on the doped samples is reported in Fig. 5 for the Y(2.5). As previously described, the fresh samples show a single intense peak and a shoulder at lower temperature (Fig. 5, trace 1). After oxidation at 700 K, the subsequent TPR featured two new peaks: the first one is strong and located at a low temperature, while the second is at a temperature close to the above-described shoulder (Fig. 4, trace 3). The shift towards low temperatures of the reduction of the solid solution after the first TPR is remarkable and strongly contrasts what is usually observed for CeO_2 where no reduction below 900 K is observed in the second TPR (9). The TPR profile shown in trace 2 of Fig. 5 was not significantly modified upon further TPR/oxidation cycles until the sample was subjected to the reduction treatment at 750 K in trace 3 of Fig. 5. In the following TPR (Fig. 5, trace 4), two broad features with maxima at 680 and 722 K were observed, suggesting that the isothermal reduction has induced a further modification of the sample. Such a modification is not observed for isothermal reduction below 750 K. The final TPR profile (Fig. 5, trace 4) was not further modified by subsequent redox cycles. In this profile, the position of the low temperature peak (Fig. 5, trace 2) is shifted to higher temperatures and the peak is somehow overlapped with the second one. Both peaks now show a comparable intensity (compare Fig. 5, trace 4 and Fig. 6, traces 3, 4, 5). The behaviour shown in Fig. 5 is common for the La(2.5) and Y(5.0). Ga(2.5) has a different evolution of the redox behaviour. The first TPR of this sample (Fig. 4, trace 7) exhibits a single peak which is significantly broader than those of all other samples. After oxidation at 700 K, in the second TPR, the initial broad peak disappears and two overlapped peaks are observed which are not further modified by the isothermal reductions. The final shape is reported in Fig. 6, trace 7. The TPR profiles of both $Ce_{0.6}Zr_{0.4}O_2$ and Y(1) also change already after the first TPR, reaching the final aspect shown in traces 1 and 2 of Fig. 6. The recycled $Ce_{0.6}Zr_{0.4}O_2$ features three broad peaks centred at 650, 720, and 840 K which indicates that part of the reduction process has shifted to lower temperatures compared to the fresh sample, while the most prominent feature is at somewhat higher temperatures (840 K compared to 822 K). A similar behaviour, e.g., a shift of the reduction temperature towards higher values

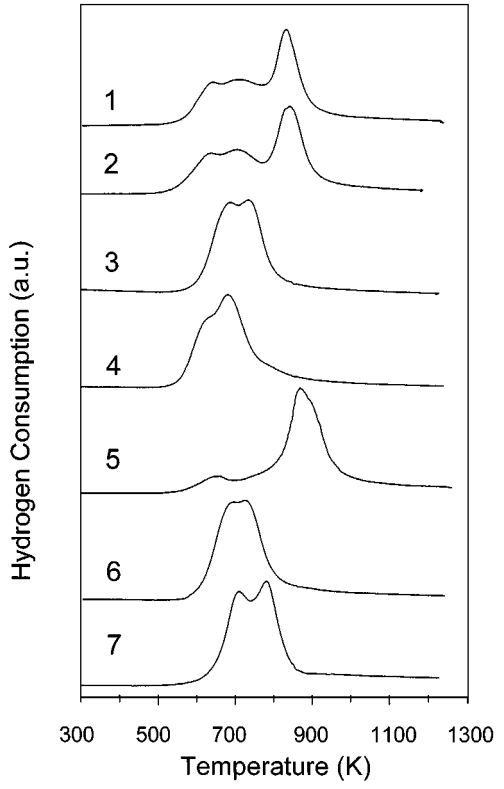

FIG. 6. Temperature programmed reduction of aged samples: (1) $Ce_{0.6}Zr_{0.4}O_2$; (2) $Ce_{0.6}Zr_{0.39}Y_{0.01}O_{1.995}$; (3) $Ce_{0.6}Zr_{0.375}Y_{0.025}O_{1.9875}$; (4) $Ce_{0.6}Zr_{0.35}Y_{0.05}O_{1.975}$; (5) $Ce_{0.6}Zr_{0.35}Y_{0.10}O_{1.95}$; (6) $Ce_{0.6}Zr_{0.375}La_{0.025}O_{1.9875}$; (7) $Ce_{0.6}Zr_{0.375}Ga_{0.025}O_{1.9875}$.

is also observed for the Y(10). In this case, the final pattern was observed already after the first TPR/oxidation cycle.

In Fig. 6, the TPR profiles of all the aged samples are compared. At a constant dopant loading (2.5 mol%), Y^{3+} leads to the most beneficial alteration of the reduction behaviour of the CeO_2–ZrO_2 mixed oxide since the reduction occurs at the lowest temperature. It is also worth of noting that, a minimum dopant concentration, e.g., 2.5 mol%, is required to modify the reduction behaviour with respect to $Ce_{0.6}Zr_{0.4}O_2$ as shown by the reduction profiles observed for the Y^{3+} doped sample (Fig. 6, traces 1–5). Increase of the Y^{3+} content favors the reducibility up to 5 mol%, while for the highest content investigated (10 mol%), the reduction temperatures increase, compared to the Y(2.5) and Y(5) samples (Fig. 6, traces 3–5).

Oxygen uptakes at 700 K measured after reduction at different temperatures are reported in Table 2. The H_2 consumption in the reduction before the oxygen uptake measurements were also evaluated. The values (not reported) correspond to the oxygen uptakes. This is in agreement with the observation that the thermal pretreatment eliminates the contributions from adsorbed species and any other artefact (9). Almost constant oxygen uptakes were measured after all the TPRs carried up to 1273 K, including those of the aged samples. The average values are reported in Table 2 for all the samples. The values measured after the isothermal reductions were obtained on the samples which were cycled for four times in the TPR/oxygen uptake experiment (compare experimental section). It is worth noting the unusually high efficiency of the Ce^{4+}/Ce^{3+} redox process which involves up to 80% mol of the Ce^{4+} present in the lattice after the reduction at 1273 K. The redox process is attributed to the Ce^{4+}/Ce^{3+} redox couple since no significant Zr^{4+} reduction was detected (9, 11, 19). The overall amount of the reducible Ce^{4+} slightly decreases as the amount of Y^{3+} increases. At 700 K, the oxidation of the reduced support is complete (8, 9) which allows to calculate from the oxygen uptakes the composition of the oxygen deficient oxides obtained in the TPR. By considering a general formula $Ce_{0.6}Zr_{0.4-x}Y_xO_y$ for the reduced Y^{3+} containing oxides, we calculate values of $y = 1.77, 1.76, 1.75, 1.74$, respectively for $x = 0$, 0.01–0.025, 0.05, and 0.10 after reduction at 1273 K. A value of 1.75 is calculated for La(2.5) and Ga(2.5). This relatively constant value may suggest that formation of a common oxygen-deficient phase might be limiting the overall degree of reduction; however, a simple coincidence due to the same TPR procedure cannot be discounted.

TABLE 2

Oxygen Uptakes at 700 K Measured over Reduced $Ce_{0.6}Zr_{0.4-x}M_xO_{2-x/2}$ and CeO_2

Sample	O_2 consumption[a] (m mol O_2 g^{-1})		(Ce^{3+}) (%)	
	(1273 K)[b]	(650 K)[c]	(750 K)[c]	(850 K)[c]
$Ce_{0.6}Zr_{0.4}O_2$	0.76 (77)	0.46 (46)	0.63 (64)	0.65 (66)
$Ce_{0.6}Zr_{0.39}Y_{0.01}O_{1.995}$	0.77 (78)	0.45 (45)	0.62 (63)	0.70 (71)
$Ce_{0.6}Zr_{0.375}Y_{0.025}O_{1.9875}$	0.76 (77)	0.57 (58)	0.64 (65)	0.68 (69)
$Ce_{0.6}Zr_{0.35}Y_{0.05}O_{1.975}$	0.74 (75)	0.54 (55)	0.62 (63)	0.67 (68)
$Ce_{0.6}Zr_{0.30}Y_{0.10}O_{1.95}$	0.68 (69)	0.17 (17)	0.46 (46)	0.59 (60)
$Ce_{0.6}Zr_{0.375}La_{0.025}O_{1.9875}$	0.76 (78)	0.58 (59)	0.63 (65)	0.67 (68)
$Ce_{0.6}Zr_{0.375}Ga_{0.025}O_{1.9875}$	0.80 (80)	0.57 (58)	0.69 (70)	0.73 (74)
CeO_2	0.50 (35)	0.01 (1)[d]		

[a] Standard deviation: ±0.01 m mol O_2 g^{-1}.
[b] TPR up to 1273 K, average value measured from all the TPR.
[c] Isothermal reduction carried out at the indicated temperature (see experimental).
[d] Isothermal reduction at 700 K.

A perusal of the oxygen uptakes measured postreduction at 750–850 K (Table 2) reveals a very high efficiency of the Ce^{4+}/Ce^{3+} redox cycle in all the samples, except for Y(10), confirming that such a high dopant level does not favor the OSC. As the reduction temperature is decreased down to 650 K, a remarkable effect of dopants on the OSC is found. There is a 20% increase of the OSC in the M^{3+} (2.5–5 mol%) doped samples compared to the $Ce_{0.6}Zr_{0.4}O_2$ and Y(1). This is an important achievement, since improvements of OSC at low temperature are highly desirable. This result is consistent with the different evolution of the TPR profiles upon the cycling of the sample in the redox cycles. It is important to note that after the final TPR, no appreciable decline of the OSC was measured in comparison to the initial TPRs up to 1273 K. For comparison, the O_2 uptakes previously measured on a CeO_2 sample (9) are also included.

Characterisation of the Aged Samples

The observed TPR behaviour indicated a significant modification of the present solid solutions induced by the redox processes. The aged samples were therefore characterized by both the Raman and XRD techniques. As shown in Fig. 1, trace 5, the powder XRD patterns reveal significant modifications of both the undoped and Y(2.5) samples as denoted by the appearance on new strong peaks at 13°–25° (2θ). Note that these low diffraction angles correspond to interplanar distances of about 3.6–6.8 nm.

The two spectra are reported here as examples; however, the same kind of modifications of the XRD patterns were observed for the other samples, suggesting that all of them have undergone a similar transformation during the redox processes. It is worth noting that the appearance of the new peaks does not produce any significant change in the positions and relative intensities of the peaks due to the *cubic* phase. Nevertheless, as shown in Fig. 7, the relative intensities of the peaks located at 13–25° (2θ) change with respect to those due to the *cubic* phase. The increase of the relative intensities of the peaks below 25° (2θ) upon increase of the Y^{3+} content suggests that the observed transformation might be favored by the presence of the trivalent dopant.

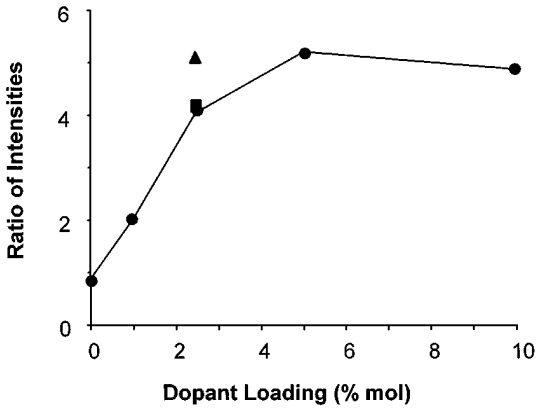

FIG. 7. Ratio of integrated intensities of the peaks at 10–25° (2θ) to the (111) reflection in the powder XRD patterns of the aged mixed oxides. (●) Y^{3+} doped samples, (■) La(2.5), and (▲) Ga(2.5).

We detected traces of Y_2O_3 in the recycled Y(10) which may account for the similar ratios of this and the Y(5) sample.

We were not able to attribute the observed XRD pattern to any known CeO_2–ZrO_2 phase. The high interplanar distances could be associated with a long-range ordering in the lattice, even if the opposite cannot be disregarded. A highly disordered phase may well present only a long range ordering.

The Raman spectra showed a net decrease of the intensity of the peak at 475 cm^{-1} attributed to the symmetrical T_{2g} stretching of the M–O bond in the fluorite lattice. This suggests that significant distortions were induced by the redox cycles in the oxygen sublattice (13).

DISCUSSION

The present results disclose important effects of the addition of trivalent cations to the $Ce_{0.6}Zr_{0.4}O_2$ solid solution. First, consistent with the ability of trivalent cations to progressively stabilize ZrO_2 in the tetragonal and cubic forms, the same effect is present in the CeO_2–ZrO_2 solid solution. We, indeed, observe that sample homogeneity and formation of a *cubic* phase is favored upon increasing the dopant content to and above 2.5 mol%. The present results strongly suggest that there is a minimum content of the dopant cation necessary to observe significant effects of the doping: both the characterization and TPR behavior reflect the equivalence of the Y(1) and the undoped sample.

Research for methods of synthesis of the CeO_2–ZrO_2 has received attention in the literature; for example, in addition to the classical coprecipitation route (20), recently the use of a high energy demanding ball milling method was proposed for the synthesis of ZrO_2 containing mixed oxides (21–23). The characterization of the fresh samples points out some important features of the synthesis of the present CeO_2–ZrO_2 solid solutions via the citrate route; high surface area, appreciable pore volume, and low calcination temperatures may be employed to obtain an efficient incorporation of both ZrO_2 and the trivalent dopant into the CeO_2 lattice. Obviously, the first two properties would be very important for precious metal deposition in the preparation of the TWCs. Recent studies highlighted the favorable effects of close contact between the metal particles and the CeO_2 support on the stabilization of metal dispersion (24). In addition, sample homogeneity and well-characterized textural properties are important factors in determining both the redox properties (9) and textural stability of these systems (25). The increase of the surface area at high Y^{3+} contents is consistent with the previous observation that the presence of a single homogeneous phase stabilizes the high surface area of the CeO_2–ZrO_2 solid solutions (25). It is worth noting that at a 2.5 mol% content of the dopant both the Y^{3+} and La^{3+} favor formation of a single phase which is not the case for the undersized Ga^{3+}. The critical radius, e.g., the cation radius which gives no cell expansion upon substitution of Zr^{4+}, is very close to that of Y^{3+} (1.1015 Å) while La^{3+} (1.18 Å) is an oversized cation. EXAFS studies suggested that oversized cations are more efficient than the undersized ones in stabilizing the ZrO_2, since the latter cations compete with Zr^{4+} for the oxygen vacancies in zirconia, resulting in sixfold oxygen coordination and a large disturbance to the surrounding next-nearest neighbors (26). Consistently, our recent EXAFS investigation disclosed a sixfold coordination around zirconia in the $Ce_{0.5}Zr_{0.5}O_2$, since the two nearest oxygens are pushed away to a nonbonding distance (19). This represents a mechanism for the release of the stress generated by insertion of the smaller Zr^{4+} into the CeO_2 lattice and at the same time it is responsible for the high oxygen mobility in the bulk by generating mobile oxygens in the lattice itself. In contrast, the Ga^{3+} which has an ionic radius of 0.62 Å (sixfold coordination) is appreciably undersized and definitely smaller than Zr^{4+} (0.72 Å in sixfold coordination). This suggests that Ga^{3+} may easily compete with Zr^{4+} for the low coordinated sites, not allowing an efficient release of the stress in the lattice. This makes formation of a single phase unfavorable.

The TPR behavior appears to be governed by both textural and structural properties, depending on whether the behavior of a fresh or a cycled sample is considered. As observed previously, an 1 mol% doping does not modify the properties of the $Ce_{0.6}Zr_{0.4}O_2$ appreciably. Consistently, these two samples present the same redox behavior. Reduction of the fresh sample substantially shows a single reduction feature, suggesting that reduction of the surface and in the bulk occur almost concurrently. Indeed, in the TPR of the fresh sample a collapse of surface area and pore filling occur which hinder the concomitant reduction of the surface. Conversely, the presence of Zr^{4+} favors the oxygen mobility in the bulk. As shown by atomistic simulation

of the solids, the energy for the $Ce^{4+} \rightarrow Ce^{3+}$ reduction in the CeO_2–ZrO_2 solid solutions is comparable to that calculated for the CeO_2 surface (27) which is in turn lower than that calculated for the reduction of CeO_2 in bulk (28). Upon the assumption that quasi-equilibrium conditions are attained during the TPR (8), due to the fast oxygen mobility in these fluorite type solids, one would expect the occurrence of two peaks, accounting for the reduction of surface and in bulk of CeO_2 and only a single feature for the CeO_2–ZrO_2 mixed oxide. This is in agreement with observations reported for the high surface area samples. Two peaks at 770 K and 1100 K are observed for CeO_2 (29) while all the single-phase mixed oxides show essentially a single reduction peak (Fig. 3). Accordingly, the small shifts of the reduction peaks observed in the fresh samples could be related to an increase of oxygen mobility induced by the dopant cation. The assumption of quasi-equilibrium conditions is indirectly supported by the observation that the final composition attained after the TPR is constant in all the samples, suggesting that formation of a nonstoichiometric oxygen-deficient phase may be limiting the overall degree of reduction.

Modification of the reduction behavior after the first TPR is an important innovative property of these materials. In the presence of H_2 as in the TPR, sintering of the high surface area samples is strongly enhanced, compared to oxidizing/inert conditions (9, 30). Accordingly, a strong crystallite growth and a decline of surface area below 10 $m^2\,g^{-1}$ were observed after these treatments (9). This produces highly crystalline, ordered solid solutions whose TPR is now characterized by two reduction features, the second one being attributed to a clustering of oxygen vacancies in the reduction process (8). In the TPR of the fresh sample, the latter process may be well hindered by the collapse of surface area and pore filling.

An important observation is the improvement of the reduction at low temperatures of the sintered samples compared to the fresh ones (Fig. 5). Such a behavior is attributed to an increase of oxygen mobility in the bulk of the solid solution induced by sintering. As shown by the Raman spectra, the local symmetry of the oxygen bonding around the zirconium cation is progressively broken, which generates mobile oxygens in the lattice (9, 19). Such a behavior is critically related to the presence of ZrO_2 in the CeO_2 lattice, since in pure high surface CeO_2 the low temperature redox processes which are related to the surface are depressed by the sintering (9, 31). In addition to this effect, the role of the bulk oxygen vacancies created by the incorporation of the trivalent dopant and their association for M^{3+} contents higher than 8 mol% cannot be discounted. Consistently, the reduction of the Y(2.5) is favored over the Y(10), even if the particle size of the former sample is smaller.

An intriguing aspect is the sample modification occurring during the isothermal reduction (Y(2.5), Y(5), and La(5)) and the TPR experiment (Ga(2.5) and La(10)). As shown by the results of the characterization of the aged samples, these treatments lead to modifications of the XRD and Raman spectra. On the basis of the present evidence, we are unable either to attribute the observed XRD pattern to any known phase or to ascertain whether phase separation has occurred. It should be noted that the CeO_2–ZrO_2 phase diagram is far from being completely understood (32, 33). For example, formation of a new cubic Φ' phase in the ZrO_2–CeO_2–$CeO_{1.5}$ ternary system and a new cubic phase for reduced CeO_2 were reported (31, 33). Nevertheless, there are indications that the formation of a new phase with the same composition might have occurred. As, in fact, diffusional phase separation triggered by the reduction has been observed in the CeO_2–ZrO_2 system only above 1473 K (34, 35). In our case, at 750 K a significant diffusion of the cationic sublattice is unfavorable. A diffusionless transformation of the mixed oxides is further substantiated by the presence of the peaks due to the initial *cubic* phase. This suggests that no enrichment in either ZrO_2 or CeO_2 occurs during the phase transformation. The increase of the relative intensity of the peaks below 25° (2θ) suggests that the phase transformation is assisted by the presence of the trivalent dopant. The undersized Ga^{3+} appears to be the most efficient cation for modifying the XRD pattern. Diffusion of small cations in a lattice is favored, compared to the oversized ones, which suggests that some dopant migration cannot be discounted.

It is important to recall, however, that despite the transformation of the mixed oxides, the degree of reduction at 1273 K is unaffected (Table 2) which may suggest some kind of structural correlation between the fresh and the aged samples.

Also worth noting is that all the samples retain very high oxygen exchange capacity at low temperatures as denoted by the TPR profiles reported in Fig. 6.

The very high values of the OSC reported in this work (Table 2) deserve some comment: in highly sintered Rh/$Ce_{0.6}Zr_{0.4}O_2$ prepared by a solid state synthesis at 1873 K (surface area $\approx$1 $m^2\,g^{-1}$) (8), the degree of reduction measured as y in $Ce_{0.6}Zr_{0.4}O_y$ was 1.76, which is almost equal to the value measured in the present work for the same composition of the solid solution. This suggests that the synthesis route does not affect the overall OSC. Conversely, the different initial texture of the solid solution modifies the reduction temperatures in the TPR and affects the behavior in the redox cycles. Consistently, $y = 1.85$ was measured after the reduction of a mixed oxide $Ce_{0.5}Zr_{0.5}O_2$, prepared both by high energy mechanical alloying (surface area 16 $m^2\,g^{-1}$) (36) and by a synthesis from alkoxide precursors (9) (surface area 64 $m^{-2}\,g^{-1}$), despite the different TPR profiles.

A major finding appears well established from the present work, e.g., that very high oxygen storage capacities

at low temperatures are obtained on these $Ce_{0.6}Zr_{0.4-x}M_xO_{2-x/2}$ systems. The insertion of the trivalent cation in an appropriate amount improves the OSC at low temperatures, compared to the undoped solid solution. Remarkably, this effect is observed in the aged samples, despite the fact that they underwent a significant sintering. High OSC at low temperatures represents a major objective of the research for the improved vehicle cold-start technology. Moreover, even if a phase modification was observed, the high OSC at low temperatures is preserved, which suggests that a limited thermal deactivation should be aspected under the real exhaust conditions. In fact, the independence of the redox behavior with respect to surface area is the most important aspect of these materials. Loss of OSC due to a drop of surface area upon thermal aging is one of the major pathways for the TWCs deactivation.

CONCLUSIONS

In summary, the present investigation has identified an important role of trivalent dopants in improving the oxygen exchange at low temperatures in the $Ce_{0.6}Zr_{0.4}O_2$ mixed oxide, compared to the undoped system. This effect is clearly shown in the sample subjected to extensive sintering induced by redox cycles. The addition of an appropriate trivalent cation affects the textural properties and, most importantly, it favors the homogeneity of the *cubic* phases. Use of citrates is indicated as an efficient route for an efficient cation insertion into the host CeO_2 lattice.

ACKNOWLEDGMENTS

We thank the National Institute of Chemistry and J. Stefan Institute (Ljubljana, Slovenia) for XRD measurements. Professor Dr. V. Kaučič (National Institute of Chemistry, Ljubljana, Slovenia), Dr. I. Kobal (J. Stefan Institute, Ljubljana, Slovenia), and Dr. A. Meden (University of Ljubljana, Slovenia) are acknowledged for many useful discussions. Magneti Marelli, D.S.S., CNR (Rome), MURST 40% (Rome), and Università di Trieste are acknowledged for financial support. One of us (P.V.) thanks the Slovenian Ministry of Science and Technology for financial support during her Ph.D. studies and the University of Trieste for a grant within the "Legge Aree di Confine" Programme.

REFERENCES

1. Taylor, K. C., "Catalysis-Science and Technology" (J. R. Anderson and M. Boudart, Eds.), Chap. 2, Springer-Verlag, Berlin, 1984.
2. Taylor, K. C., *Catal. Rev.-Sci. Eng.* **35**, 457 (1993).
3. Golunski, S. E., Hatcher, H. A., Rajaram, R. R., and Truex, T. J., *Appl. Catal. B. Environ.* **5**, 367 (1995).
4. Schmieg, S. J., and Belton, D. N., *Appl. Catal. B. Environ.* **6**, 127 (1995).
5. Usmen, R. K., Graham, G. W., Watkins, W. L. H., and McCabe, R. W., *Catal. Lett.* **30**, 53 (1995).
6. Bensalem, A., BozonVerduraz, F., Delamar, M., and Bugli, G., *Appl. Catal. A. Gen.* **121**, 81 (1995).
7. Zamar, F., Trovarelli, A., de Leitenburg, C., and Dolcetti, G., *J. Chem. Soc. Chem. Commun.*, 965 (1995).
8. Fornasiero, P., Di Monte, R., Ranga Rao, G., Kašpar, J., Meriani, S., Trovarelli, A., and Graziani, M., *J. Catal.* **151**, 168 (1995).
9. Fornasiero, P., Balducci, G., Di Monte, R., Kašpar, J., Sergo, V., Gubitosa, G., Ferrero, A., and Graziani, M., *J. Catal.* **164**, 173 (1996).
10. Fornasiero, P., Balducci, G., Kašpar, J., Meriani, S., Di Monte, R., and Graziani, M., *Catal. Today* **29**, 47 (1996).
11. Ranga Rao, G., Fornasiero, P., Di Monte, R., Kašpar, J., Vlaic, G., Balducci, G., Meriani, S., Gubitosa, G., Cremona, A., and Graziani, M., *J. Catal.* **162**, 1 (1996).
12. Meriani, S., and Spinolo, G., *Powder Diffract.* **2**, 255 (1987).
13. Yashima, M., Arashi, H., Kakihana, M., and Yoshimura, M., *J. Am. Ceram. Soc.* **77**, 1067 (1994).
14. Courty, P., Ajot, H., Marcilly, C., and Delmon, B., *Powder Technol.* **7**, 21 (1973).
15. Yashima, M., Morimoto, K., Ishizawa, N., and Yoshimura, M., *J. Am. Ceram. Soc.* **76**, 2865 (1993).
16. Yashima, M., Morimoto, K., Ishizawa, N., and Yoshimura, M., *J. Am. Ceram. Soc.* **76**, 1745 (1993).
17. Yashima, M., Ishizawa, N., and Yoshimura, M., *J. Am. Ceram. Soc.* **75**, 1541 (1992).
18. Graham, G. W., Weber, W. H., Peters, C. R., and Usmen, R. K., *J. Catal.* **130**, 310 (1991).
19. Vlaic, G., Kašpar, J., Geremia, S., Fornasiero, P., and Graziani, M., *J. Catal.* **168**, 386 (1997).
20. de Leitenburg, C., Trovarelli, A., Llorca, J., Cavani, F., and Bini, G., *Appl. Catal. A. Gen.* **139**, 161 (1996).
21. Chen, Y. L., Qi, M., Yang, D. Z., and Wu, K. H., *Mater. Sci. Eng. A-Struct. Mater.* **183**, L9 (1994).
22. Michel, D., Mazerolles, L., Berthet, P., and Gaffet, E., *J. Am. Ceram. Soc.* **76**, 2884 (1993).
23. de Leitenburg, C., Trovarelli, A., Zamar, F., Maschio, S., Dolcetti, G., and Llorca, J., *J. Chem. Soc. Chem. Commun.*, 2181 (1995).
24. Brogan, M. S., Dines, T. J., and Cairns, J. A., *J. Chem. Soc. Faraday Trans.* **90**, 1461 (1994).
25. Sun, Y., and Sermon, P. A., *J. Mater. Chem.* **6**, 1025 (1996).
26. Li, P., Chen, I. W., and Penner-Hahn, J. E., *J. Am. Ceram. Soc.* **77**, 118 (1994).
27. Balducci, G., Islam, M. S., Gale, J. D., Kašpar, J., and Graziani, M., *J. Phys. Chem. B* **101**, 1750 (1997).
28. Sayle, T. X. T., Parker, S. C., and Catlow, C. R. A., *Surface Sci.* **316**, 329 (1994).
29. Yao, H. C., and Yu Yao, Y. F., *J. Catal.* **86**, 254 (1984).
30. Perrichon, V., Laachir, A., Abouarnadasse, S., Touret, O., and Blanchard, G., *Appl. Catal. A. Gen.* **129**, 69 (1995).
31. Perrichon, V., Laachir, A., Bergeret, G., Frety, R., Tournayan, L., and Touret, O., *J. Chem. Soc. Faraday Trans.* **90**, 773 (1994).
32. Meriani, S., *Mater. Sci. Eng. A-Struct. Mater.* **71**, 365 (1985).
33. Otsuka-Yao, S., Morikawa, H., Izu, N., and Okuda, K., *J. Japan Inst. Metals* **59**, 1237 (1996).
34. Heussner, K. H., and Claussen, N., *J. Am. Ceram. Soc.* **72**, 1044 (1989).
35. Zhy, H., Hirata, T., and Muramatsu, Y., *J. Am. Ceram. Soc.* **75**, 2843 (1992).
36. Zamar, F., Trovarelli, A., de Leitenburg, C., and Dolcetti, G., *Stud. Surf. Sci. Catal.* **101**, 1283 (1996).